JOURNAL of
MATERIALS and MECHATRONICS:A

e-ISSN 2717-8811
JournalMM, 2023, 4(2), 542-560
https://doi.org/10.55546/jmm.1326482

Araştırma Makalesi / Research Article

Preparation of Diatomite-Chitosan Composites for Loading and Release of Diphenhydramine HCl

Zeynep ÖZKAN[1], Muhammet Davut ARPA[2*], Melih ÖZÇATAL[3], Hakan ÇİFTÇİ[4**]

[1]Afyon Kocatepe University, Graduate School of Natural and Applied Sciences, Department of Nanoscience and Nanotechnology, Afyonkarahisar, Türkiye,
ORCID ID: https://orcid.org/0000-0003-2793-157X, zeyyozkan26@gmail.com
[2]Istanbul Medipol University, School of Pharmacy, Department of Pharmaceutical Technology, Istanbul, Türkiye,
ORCID ID: https://orcid.org/0000-0001-9290-2404, mdarpa@medipol.edu.tr
[3]Afyon Kocatepe University, Faculty of Technology, Department of Mechatronics Engineering, Afyonkarahisar, Türkiye,
ORCID ID: https://orcid.org/0000-0002-0831-9038, mozcatal@aku.edu.tr
[4]Afyon Kocatepe University, Faculty of Engineering, Department of Mining Engineering, Afyonkarahisar, Türkiye,
ORCID ID: https://orcid.org/0000-0001-7910-7350, hakanciftci86@gmail.com

Geliş/ Received: 12.07.2023; **Kabul / Accepted:** 03.12.2023

ABSTRACT: Diatomite ores have great potential as an adsorbent and drug carrier system due to their natural abundance, biocompatible, and high surface area. In the first stage of this study, raw diatomite ore was enriched by grinding and calcination processes. As a result of the enrichment process, the surface area was found to be 21.7 m^2/g for raw diatomite and 75.1 m^2/g for calcined diatomite. Subsequently, a series of diatomite-chitosan composites with different composition ratios were produced. Then, the loading (adsorption) performances of diphenhydramine hydrochloride (DPH), an antihistaminic agent, were investigated on the prepared composites. The highest loading capacity was 91.1 mg/g, and the lowest loading capacity was 48.8 mg/g in the prepared DPH-loaded formulations. After DPH loading studies, DPH release profiles (desorption) and release kinetics from composites were investigated. As a result of *in vitro* release studies, it was observed that formulations containing chitosan polymer had slower release than chitosan free formulations. It was determined that the formulations had a cumulative release in the 70-90% range, and the release processes were completed between 45-90 minutes. *In vitro* release profiles of the prepared formulations were compatible with Higuchi kinetics.

Keywords: Diatomite, Chitosan, Diphenhydramine, Release kinetic.

*Sorumlu yazar / Corresponding author: *mdarpa@medipol.edu.tr **hakanciftci86@gmail.com

Bu makaleye atıf yapmak için /To cite this article

Özkan, Z., Arpa, M.D., Özçatal, M., Çiftçi, H. (2023). Preparation of Diatomite-Chitosan Composites for Loading and Release of Diphenhydramine HCl. Journal of Materials and Mechatronics: A (JournalMM), 4(2), 542-560.

1. INTRODUCTION

For the active substance released in drug delivery systems to be beneficial, it must remain within the therapeutic range. In classical drug delivery methods, repeat doses are needed to ensure the therapeutic dose. Controlled release systems can reduce these dose repetitions and side and toxic effects. The selection of an appropriate and effective drug delivery system depends on its biocompatibility, loading capacity, release rate, safety, and cost of production (Ibrahim et al., 2021). One of the popular examples of materials with these properties is natural or synthetic silica and silicate-based materials. In the last decade, porous and micro-nano-sized silicates have attracted significant attention in pharmaceutical applications due to their excellent biocompatibility, high surface area, thermal stability, chemical inertness, and diffusion-controlled drug release mechanisms. In the last decade, porous and micro-nano-sized silicates have attracted much attention in pharmaceutical applications, especially as drug delivery systems. Because these substances have a high surface area, are chemically and physically stable, and are also biocompatible. For example, natural nanoporous silicates such as diatomite and natural zeolite are more cost-effective than synthetic porous silica-based materials (Zhang et al., 2013; Ibrahim et al., 2021). Micro- and nano-scale drug delivery systems have significantly affected the pharmaceutical industry by minimizing the disadvantages of drugs, such as short half-life, poor stability, and side effects (Çiftçi et al., 2020).

Diatomaceous earth, also known as diatomite, is a fossil material of sedimentary origin, formed over centuries by the siliceous skeleton (frustule) of single-celled micro-algae in water, deposited at the bottom of lakes or found in marine environments. Diatomite morphology consists of particles of sizes ranging from 2 μm to 2 mm. Particle size distributions may vary according to the type and size of diatoms, their shells, and clay and sand inclusions. The bulk density of diatomite is between 0.51-0.55 g/cm^3) and the specific gravity of 2.55 g/cm^3 (Reka et al., 2021). Diatomite frustules can have a large surface area of up to 200 m^2/g (Wang et al., 2013; Rea et al., 2014). Diatomite, whose main component is amorphous silica, may contain organic compounds from the environment and impurities such as metal oxides (MgO, Al_2O_3, Fe_2O_3). Therefore, raw diatomite may need to be purified first. For this, processes such as thermal calcination and washing with HCl are used (M Rosenholm et al., 2011; Taş and Çetin, 2012). Physical (gravity methods, separation according to particle size, sedimentation) and chemical enrichment (acid leaching, calcination) methods can be used in diatomite enrichment. Physical enrichment methods are suitable for some diatomite ores and are ineffective in increasing the specific surface area. In this case, chemical enrichment methods can be used. Organic impurities accumulated in the pores of diatomite can only be removed by chemical methods. The leaching method can remove Organic substances by dissolving them, but this method is costly. The calcination process is the cheapest and most efficient method to enrich ores such as diatomite and increase the surface area. It is known that the total potential diatomite reserve in the world is 2 billion tons, and it is approximately 125 million tons in Turkey (Ruggiero et al., 2014). Due to its widespread availability in many parts of the world, its high thermochemical stability, low density, high adsorption capacity, non-toxicity, and excellent biocompatibility, it interests researchers in many areas. Diatomite is a promising adsorbent material thanks to the pores on the frustule surface and the pores between the frustules (Wang et al., 2013). In a study the removal of some heavy metal ions such as Al^{+3}, Ba^{+2}, Cd^{+2}, Cr^{+3}, Cu^{+2} by taking advantage of the excellent adsorption capacity of diatomite was investigated. It is observed that the maximum removal percentage of many heavy metal ions at pH 4 (M Rosenholm et al., 2011). At the same time, diatomite is of interest as a potential drug carrier in pure or modified form. For example, in a study diclofenac sodium was adsorbed on a modified diatomite sample and the formulation showed a release over 8 h, further indicating the

potential safety of diatomite in their *in vivo* toxicity test results on mice (Taş and Çetin, 2012). In another study, different concentrations of chemically modified diatomite nanoparticles were incubated in cancer cells and homogeneous distribution of nanoparticles in the cytoplasm and nucleus in imaging analysis was observed (Ruggiero et al., 2014). Diatom microalgae drug carrier systems was developed for topical delivery of naproxen. In cytotoxicity studies, it has been shown that both the diatom and the carrier system are not cytotoxic (Vona et al., 2023). In a study, a diatomite-based sponge was developed to prevent excessive bleeding. With the biocompatibility studies performed, the blood compatibility, cytocompatibility, and histocompatibility of the system were tested separately by in vitro or in vivo studies. It was determined that these diatomite-based carrier systems were highly biocompatible due to a 5% of hemolysis rate, and 90% of cell viability, as well as not affecting the proliferation and the growth of tissue cells, and not causing any inflammation (Yang et al., 2021). Studies showed that phase transformations in diatomite occur from 600 to 1200°C, however, critical changes in the opal phase were reported to be observed between 1000 and 1200°C (Reka et al., 2021).

Polymers play an essential role as carriers in the design of efficient drug delivery systems due to their stability, high drug-loading capacity, and providing controlled drug release (Vilar et al., 2012; Abdel-Bary et al., 2020). Natural chitosan shows promising results in drug delivery systems among the available polymers. Chitosan, obtained by deacetylation of chitin, mainly found in shellfish, is the second most abundant polymer after cellulose. Chitosan technically have high reactivity, high stability, high biocompatibility, non-toxicity, and high biodegradability (Tian et al., 2020; Arpa et al., 2023). All these properties are helpful for the production of chitosan as a potential carrier with various types of silica and silicate-based structures. Thanks to this integration, the physicochemical properties of chitosan combined with diatomaceous earth improve (Burkhanova et al., 2000; Akyuz et al., 2017). According to a reported study, curcumin loaded on chitosan-silica nanoparticles and 48-hour release was observed. It is stated that it promises as a pH-dependent drug-releasing molecule (Gaware et al., 2019).

Histamine is a chemical mediator that mediates allergic and inflammatory reactions, gastric acid secretion, and neurotransmission in specific brain regions. Various drugs, such as dimenhydrinate, thyroxine, pheniramine, and diphenhydramine, have been used to abolish the effects of histamine by blocking histamine receptors. Diphenhydramine hydrochloride (DPH) is a potent antihistamine active ingredient (H_1 receptor blocker) with antiemetic, sedative, and anticholinergic effects. DPH causes strong side effects such as dry mouth and throat, tachycardia, pupillary dilation, urinary retention, constipation, motor impairment, hallucinations, and delirium at high doses. The controlled release has been proposed as a promising method to reduce the reported side effects of the active ingredient using innovative carriers. Various methods have been developed to minimize these side effects and provide a controlled release of DPH (Ghebaur et al., 2012; Rezaeifar et al., 2016).

In this study, raw diatomite was first enriched by calcining and then characterized. Later, drug carrier systems were obtained using calcined diatomite and chitosan. A total of six different formulations were produced from different diatomite and chitosan composition ratios and different DPH loading amounts. The effect of delivery systems on DPH release characteristics was evaluated by examining their drug release profiles. Release data were analyzed using Zero order, First order, Higuchi, Hixson-Crowell, and Korsmeyer Peppas kinetics.

2. MATERIALS and METHODS

2.1 Materials

Raw diatomite samples were collected from Afyonkarahisar Seydiler District, diphenhydramine HCl, hydrochloric acid, potassium dihydrogen phosphate, o-phosphoric acid, and acetonitrile were purchased from Sigma-Aldrich, chitosan (low molecular weight, deacetylation degree >90) was purchased BBI Life Scineces, sodium hydroxide was purchased from Merck, and acetic acid (glacial) was purchased from Carlo Erba. All used chemicals were pharmaceutical grade.

2.2 Methods

2.2.1 Purification of diatomite

The purification process was carried out to increase the diatomite's surface area and purify it from its impurities. For this, three stages of crushing and grinding were carried out to reduce the diatomite's particle size. The large-grained diatomite was first fed into the laboratory jaw crusher, the primary crusher, and then the roller crusher, the secondary crusher. The crushed diatomite was then ground in a ring mill for 2 min. After that, the ground diatomite was subjected to drying and calcination processes. It was kept in an oven at 105°C for 24 h for the drying process. Then, it was held in a laboratory-type ash oven at 550°C for 4 h to be calcined. Temperatures between 500-600 ºC are generally used to remove organic substances. While it may not be fully effective at lower temperatures, structural deterioration may occur in the inorganic material at higher temperatures.

2.2.2 Characterization studies of raw and purified diatomite

The raw and purified diatomite samples were dried at 105ºC for 24 hours and ground in a ring mill for 2 minutes. Then, X-ray diffraction (XRD) spectra were obtained with the Shimadzu XRD-6000 instrument with Cu-Ka radiation at a wavelength of λ: 1.54184 Å. The samples were scanned in the 2-70º angle range. The chemical composition of the samples, which were subjected to the same pre-treatment, was also determined elementally with the XRF (Rigaku ZXS Primus II) device. LEO 1430 VP model SEM device was used to determine the topographic features of the dried and ground samples. The specific surface areas of the raw and calcined diatomite samples were calculated by the Brunauner-Emmett-Teller (BET) equation, which is based on the calculation of the amount of gas required to cover the sample surface with a single molecular layer. The size distribution of the pores was obtained from the desorption isotherm data using the Barrett, Joyner, and Halenda (BJH) method. To this end, Micromeritics brand Gemini VII 2390t model device based on nitrogen gas adsorption technique in a liquid nitrogen environment at -196ºC was used. Particle size distributions were determined using the Malvern Mastersizer 2000 instrument, and the procedures in our previous work were followed for the analysis (Çiftçi et al., 2020). For zeta potential (ζ) analysis, Malvern brand Nano-Z model zeta-meter device was used, and the procedure in our previous studies was followed for the analysis (Çiftçi et al., 2020).

2.2.3 Preparation of DPH loaded diatomite-chitosan composites

First, a 2% aqueous acetic acid solution containing 1 mg/mL of active ingredient (DPH) was prepared. 250 mL of this prepared stock solution was used to prepare each formulation. A certain amount of diatomite was added to 250 mL of stock solution and stirred for 1 h at 55°C in a magnetic stirrer. Then, the amount of chitosan determined in the formulations was added to the solution. Chitosan-containing solutions were stirred on a magnetic stirrer at 55°C for 24 h. The product obtained at the end of the process was dried in an oven at 55°C for 24 h. The same procedures were repeated for all formulations. A temperature value of 55oC was used to increase the solubility of

chitosan, to avoid damaging the drug molecules at higher temperatures, and to also dry the formulation. The composition ratios of the prepared formulations (Table 1) were determined according to the general literature review.

Table 1. The composition ratios of the prepared formulations.

Formulation	DPH/Carrier material	Amount of diatomite (mg)	Chitosan ratio (%) (according to the total amount of carrier)	1000 mg/L DPH solution (mL)
F1	1/10	2500	0	250
F2	1/10	1625	35	250
F3	1/10	1875	25	250
F4	1/7.5	1875	0	250
F5	1/7.5	1218.75	35	250
F6	1/7.5	1406.25	25	250

2.2.4 FT-IR analysis

The functional groups and FT-IR spectra of the purified diatomite, chitosan, DPH and the composite formulations were examined in a Perkin Elmer device in the 400-4000 cm^{-1} range.

2.2.5 Quantification of DPH and loading capacity

Eight different DPH solutions at specific concentrations were prepared from 100 mcg/mL of DPH stock solution by diluting them with distilled water, and their measurements were performed using a HPLC (Agilent 1100) device. The calibration equation and determination coefficient (r^2) were determined by drawing the calibration graph with the data obtained (Figure 1). To determine the maximum loading capacities, 60 mg of powder formulations was dispersed in 200 mL of distilled water and after 12 h the samples were taken, filtered and analyzed by HPLC device.

An Agilent 1100 HPLC device was used in the HPLC method developed to determine diphenhydramine HCl (DPH). Validation parameters such as linearity, reproducibility, precision, limit of quantification (LOQ), and limit of detection (LOD) were evaluated. A C18 column (GC Sciences, InterSustain C18, 150*4.6 mm, 5 μm) was used for analysis. 35% aqueous acetonitrile phosphate buffer solution (pH: 3) was used as the mobile phase. The flow rate was 1.2 mL/min, the wavelength was 227 nm, the injection volume was 20 μL, and the column temperature was 25°C. A stock solution was prepared by dissolving DPH in 35% aqueous acetonitrile at a 100 μg/mL concentration. Samples were prepared from this stock solution by making dilutions with 35% aqueous acetonitrile solution in the 1-30 μg/mL range. All samples were filtered using a membrane filter (pore size of 0.2 μm).

2.2.6 In vitro release studies

The release study of drug-loaded formulations was performed using UPS apparatus I - basket method (Figure 1). *In vitro* release profiles of the composites were determined in simulated gastric fluid (80 mL of 1.0 N HCl, 2.0 g NaCl, q.s. 500 mL purified water: pH: 1.2) release media. First, the formulations containing 25 mg of diphenhydramine HCl (DPH) were weighed. It was filled into hard gelatin capsules numbered 0, as suitable for the bulk density and amount of the material. The weights of the filled capsules were recorded. The speed of the dissolution device was set to 50 rpm and the temperature to 37±1°C. Vessels were filled with 900 mL of the simulated gastric fluid. At the specified time intervals (5, 15, 30, 45, 60, 75, 90, 120, 150, and 180 min), 1 mL sample was taken

and filtered through a membrane filter (pore size of 0.2 μm) and transferred to vials. The same amount of fresh medium was added to the vessels. Samples were analyzed in the HPLC device at 227 nm. The study was performed in triplicate for each formulation, and the mean values of the results were recorded.

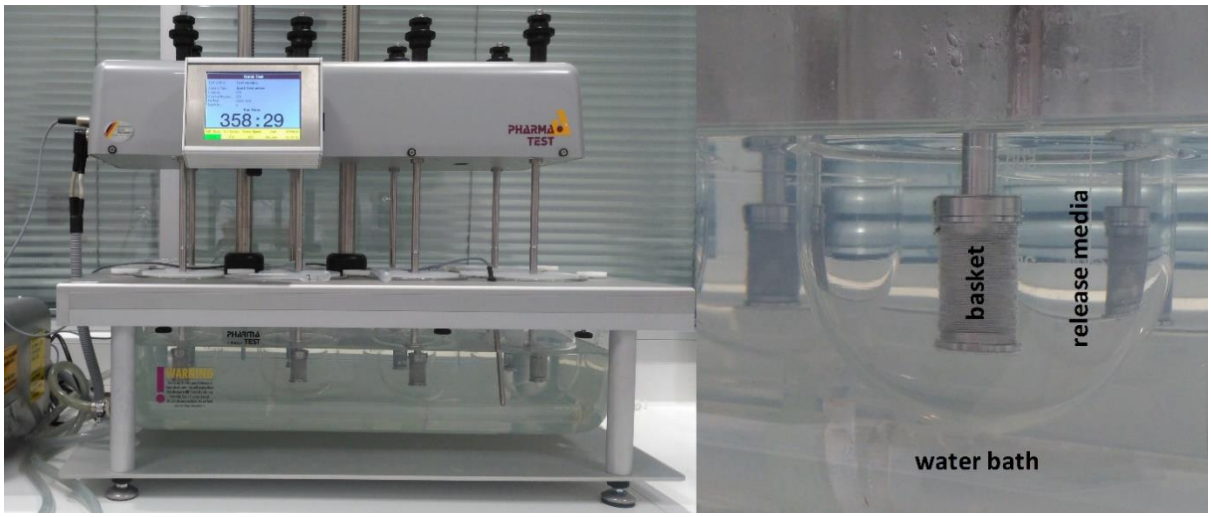

Figure 1. Dissolution device and release medium used in release studies.

In order to explain the kinetics of DPH release from chitosan-diatomite composites, the results of the release studies were analyzed using kinetic models. Equations of the models used (Equations 1-5) are given below. In addition, whether there was a similarity between the release characteristics of the formulations was determined by the f2 similarity factor. f2>50 was evaluated being similarity of the DPH release profiles (Arpa et al., 2021).

Zero order equation

$$M_t/M_\infty = k_0.t \quad (1)$$

First order equation

$$\ln(1-(M_t/M_\infty)) = -k_1.t \quad (2)$$

Higuchi equation

$$M_t/M_\infty = k_H.t^{1/2} \quad (3)$$

Hixson-Crowell equation

$$1-(1- M_t/M_\infty)^{1/3} = -k_{HC}.t \quad (4)$$

Korsmeyer-Peppas equation

$$M_t/M_\infty = k_{KP}(t)^n \quad (5)$$

where M_t and M_∞ are drug release at "t" and equilibrium time, respectively. k_0, k_1, k_H, k_{HC}, k_{KP} are the respective release rate constants. n is a constant describing the release mechanism.

Mechanisms corresponding to the "n" value have been determined for polymeric-controlled release systems. Dissolution of the drug delivery system when n>1, controlled release through

diffusion from the polymer matrix when n<0.5, and drug diffusion and dissolution of the carrier system at the same time when 0.5<n<1 are in question (Kevadiya et al., 2012; Luo et al., 2016).

2.2.7. Statistical analyzes

For the evaluation of the data obtained, statistical analyzes were made by applying Student's t-test. $p<0.05$ was accepted as statistically significant.

3. RESULTS and DISCUSSION

3.1 Characterization Studies

The XRD spectrum showing the crystal structure of diatomite is given in Figure 2. The broad band observed at 2θ=22° in the spectrum indicates the presence of amorphous silica, forming the diatomite's characteristic structure. Apart from the peak showing the presence of amorphous silica, a sharp peak indicating the presence of another mineral could not be detected in the spectrum.

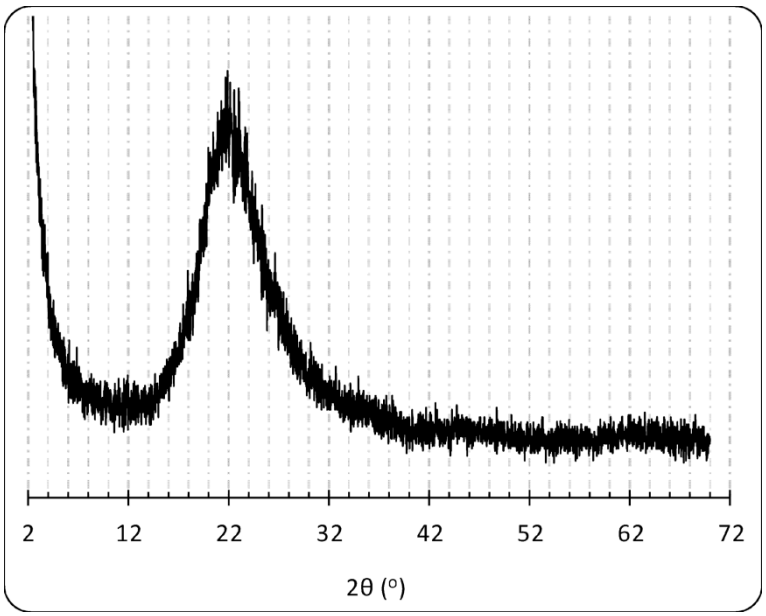

Figure 2. XRD spectrum of the diatomite sample.

Diatomites'chemical composition and crystal structure play an essential role in drug release. In the XRF analysis of the diatomite, the results of which are given in Table 2, SiO_2 was observed as the primary component with a ratio of 94.5%. This result is in agreement with the XRD data (Moradi and Yıldız, 2021). The 3.3% increase in glow loss can be attributed to organic impurities precipitated in the diatomite pores.

Table 2. Chemical analysis (XRF) results of diatomite sample.

Component	SiO_2	Al_2O_3	CaO	Fe_2O_3	K_2O	Na_2O	MgO	LOI
Amount (wt. %)	94.51	0.98	0.42	0.30	0.17	0.08	0.08	3.3

LOI: Loss of ignition

The surface morphology of the diatomite was investigated based on SEM images (Figure 3). Diatomite, which has a highly porous structure, also appears to contain large volumes of voids after calcination. Having these properties makes diatomite a potential material in drug release applications. Diatomite grains were found to be circular, elliptical, and elongated. There was a heterogeneous

population of structures that differ in both size and shape. It can be seen from Figure 3(a,b) that the micro and submicron pores and crevices in the form of the raw diatomite are primarily open and are not closed much by organic materials. A 3.3% mass loss in XRF analysis also supported this. Figure 3(c,d) showed that the submicron pores were open in some grains after calcination; that is, the organic structures in these pores were removed by calcination.

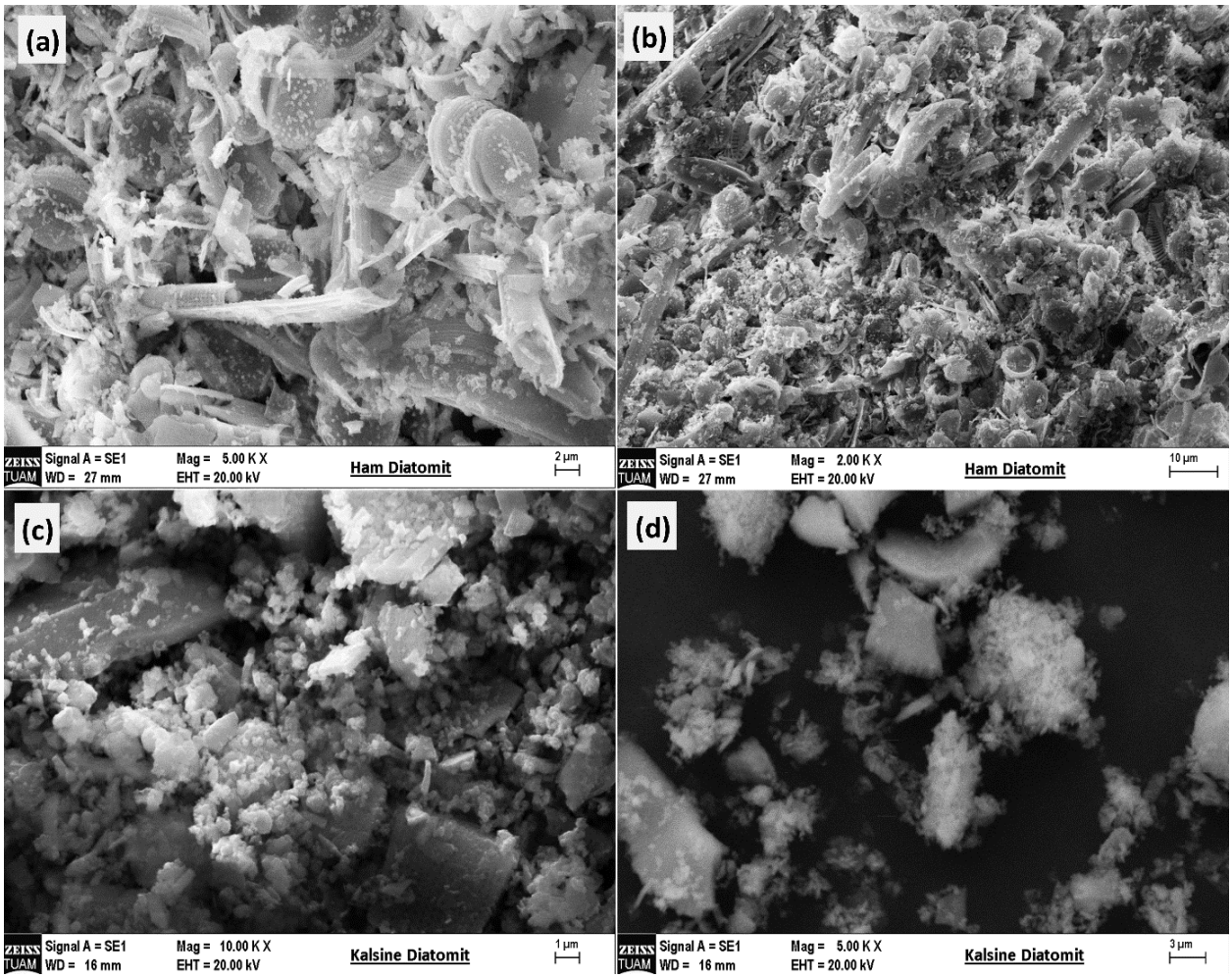

Figure 3. SEM images of raw (a,b) and calcined (c,d) diatomite.

Table 3 gives the raw and calcined diatomite properties determined by the N_2 sorption method. After the calcination process, the morphological structure of the diatomite did not fundamentally change, but it was observed that the surface area increased significantly as a result of the opening of Si-O-Si bridges on the diatomite spine surface and the removal of organic impurities (Fowler et al., 2007). The literature has reported that temperatures above 1600°C close the siloxane bridges (Yusan et al., 2012). In this study, due to the calcination carried out at 550°C, an almost 3-fold increase was observed in the pore volume determined by the BJH method, from 0.24 cm^3/g to 0.76 cm^3/g. It was concluded that the calcination processes performed at low temperatures increased the surface area and pore volume. Additionally, the pore size of the diatomite sample was around 50 nm, that is, it was mesoporous. It is known that the mesoporous structure is a useful feature for controlled drug release systems as it slows down the release (Çiftçi et al., 2020).

Table 3. Textural properties of the diatomite samples.

Sample	BET surface area (m^2/g)	Total volume of pores, with BJH ads. (cm^3/g)	Average pore diameter, with BJH ads. (nm)
Raw diatomite	21.69	0.24	52.18
Calcined diatomite	75.11	0.76	49.0

N_2 adsorption-desorption isotherms of raw and calcined diatomite are given in Figure 4(a). As can be seen in the graph, the isotherm of calcined diatomite belongs to type III with an H_3 hysteresis loop according to the International Union of Pure and Applied Chemistry (IUPAC) classification, which corresponds to the characteristic curves of mesoporous and macroporous materials (Yusan et al., 2014; Zheng et al., 2019). Such isotherms are associated with the formation of aggregates with plate-like fragments. When P/P_0 is close to 1, it shows that the adsorption in the macropores occurs at the maximum level (Tsai et al., 2006; Gârea et al., 2016; Silvestri et al., 2017). The BJH pore size distributions of raw and calcined diatomite are given in Figure 4(b). It can be said that the diatomite samples have a macroporous (pore diameter > 50 nm) structure according to the classification according the size of the pores recommended by the International Union of Pure and Applied Chemistry (IUPAC). Both diatomite samples have a heterogeneous pore diameter distribution with pore distributions below 125 nm. However, the increase in the pore volume of the calcined diatomite is seen. From this, it is understood that the macro and mesopores are opened after the calcination process. BJH pore size distributions also overlap with the data obtained by BET analyses (Table 3).
Zeta potential (ζ) measurements were performed in 10^{-3} M NaCl solution with 0.01% solid ratio. The ζ values of the diatomite surface at different pH values are given in Figure 4(c). It is seen that the ζ changed according to the pH value of the environment. As is known, the ζ of diatomite particles is negative over a wide pH range. Therefore, the surface of diatomite particles is naturally negatively charged (Gao et al., 2005). While the ζ value was -14.4 mV at the lowest pH value (1.9), the ζ value was measured as -33.8 mV when the pH value was 12. It is understood from the graph that the negative charge decreases with increasing pH.

The particle size distributions of the raw and calcined diatomite are given in Figure 4(d). As seen in the graph, it was determined that the particle sizes of raw and calcined diatomite samples were between 1.5-50 μm, and they had a homogeneous size distribution. However, it was observed that there was a slight increase in the particle size distribution after the calcination process. The reason for this can be explained by the fact that tiny particles physically adhere to each other and agglomerate after the calcination process (Ediz et al., 2010). When the d_{10}, d_{50}, and d_{90} values of diatomite samples were compared, the d_{50} value of natural diatomite was 7.7 μm, while the d_{50} value of calcined diatomite was 8.9 μm. Similarly, the d_{90} value of natural diatomite was determined as 20.3 μm, and the d_{90} value of calcined diatomite was 21.3 μm by grain size analysis (Table 4). This means the diatom structure shrinks and agglomerates due to removing organic matter and moisture after calcination, as expressed in the particle size distribution graphs.

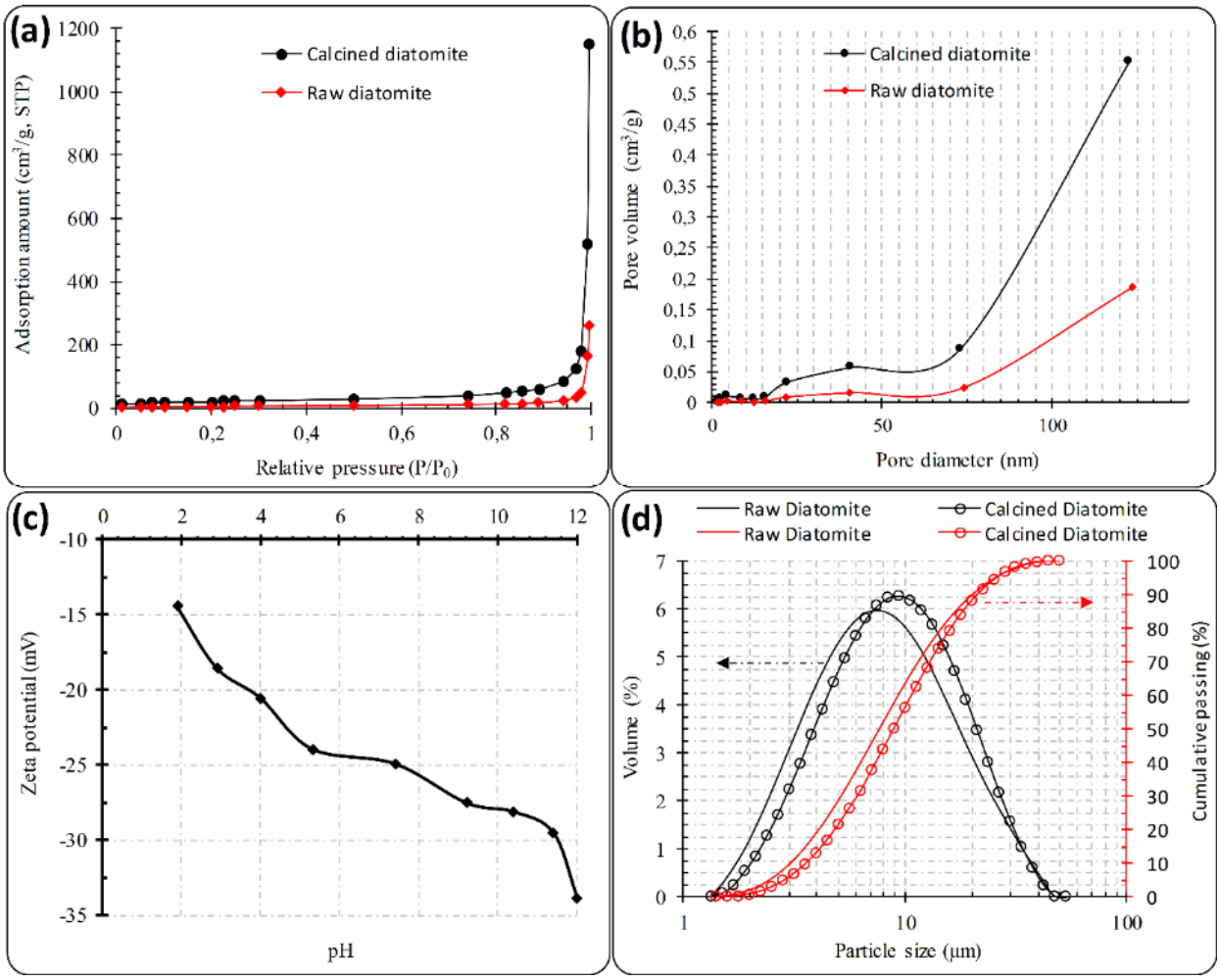

Figure 4. (a); N_2 sorption isotherms, (b); pore size distributions, (c); zeta potential with respect to pH, and (d); particle size distributions of the diatomite samples.

Table 4. Particle size distributions of the raw and calcined diatomite samples.

	Raw diatomite	Calcined diatomite
d_{10} (µm)	3.1	3.6
d_{50} (µm)	7.7	8.9
d_{90} (µm)	20.3	21.3

3.2 FT-IR Analysis

The functional groups of the composite components and all formulations were determined by FT-IR spectra (Figure 5). It is seen that the calcined diatomite revealed three characteristic broad bands: 1065 cm^{-1}, 797 cm^{-1}, 454 cm^{-1}. These peaks are assigned to the symmetric stretching vibration of the Si-O-Si group, the Si-OH bending vibration and the characteristic band of the Si-O-Si bond, respectively. The peak at 1624 cm^{-1} wavelength can be assigned to the H-OH bend, which is a weak bend (Gültürk and Güden, 2011). The band between 3600-3000 cm^{-1} seen in the chitosan FT-IR spectrum corresponds to the stretching of the hydroxyl (OH) groups and was a wide band due to hydrogen bonds (Zheng and Wang, 2009). The 2948 cm^{-1} and 2861 cm^{-1} absorption bands represent C-H symmetrical and asymmetrical stresses, respectively. 1645 cm^{-1} C=O stretching (Amine I), 1636 cm^{-1} and 1318 cm^{-1} C-N stretching (Amine III), 1582 cm^{-1} NH bending, 1377 cm^{-1} CH bending, 1028

cm^{-1} C-O stretching (Queiroz et al., 2014; Thakur et al., 2016). The peak at a wavelength of 891 cm^{-1} represents the saccharide groups in chitosan (Thakur et al., 2016). In the spectrum of diphenhydramine, aromatic C-H stretching, amine C-N stretching and ether C-O stretching were observed in the absorption bands of 3033 cm^{-1}, 1172 cm^{-1} and 1108 cm^{-1}, respectively (Abbas et al., 2020). In addition, the peaks corresponding to wavelengths of 2953 cm^{-1} and 1455 cm^{-1} represent stretching vibrations of the CH bond in CH_2 groups (Zargarian et al., 2015). Vibrations at 756 cm^{-1}, 714 cm^{-1} represent the C-H deformation of phenyl outside the aromatic benzene ring (Ly et al., 2017).

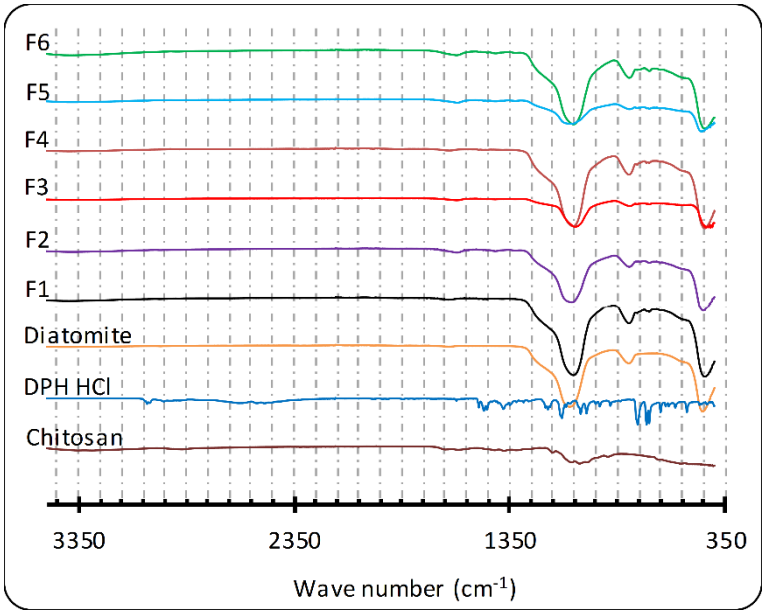

Figure 5. FT-IR spectra of the samples.

The bands around 1582 cm^{-1} belonging to chitosan disappeared in the formulations. This indicates that the peaks of the weaker amide and amine groups of chitosan compared to diatomite are absorbed by the dominant peaks of the diatomite (Wu et al., 2016). Dominant peaks of DPH molecules were also detected in the formulations. This proves that DPH molecules are adsorbed on the carrier composite. It was observed that the Si-O stretching vibration intensity in the 1065 cm^{-1} band of the diatomite and the Si-OH bending vibration intensity in the 797 cm^{-1} band decreased due to the addition of chitosan.

3.3 Calibration Curve and Srug (DPH) Loading Capacities

The correlation coefficient was found to be 0.99 according to the HPLC method developed (Figure 6). The high reproducibility and precision of the DPH assay method were demonstrated by the obtained coefficients of variation of less than 2% (data not shown). The formulations with the highest and the lowest loading capacity were determined as F1 and F5, respectively (Table 5). It was observed that the presence of chitosan in the prepared formulations caused a decrease in the DPH loading capacity.

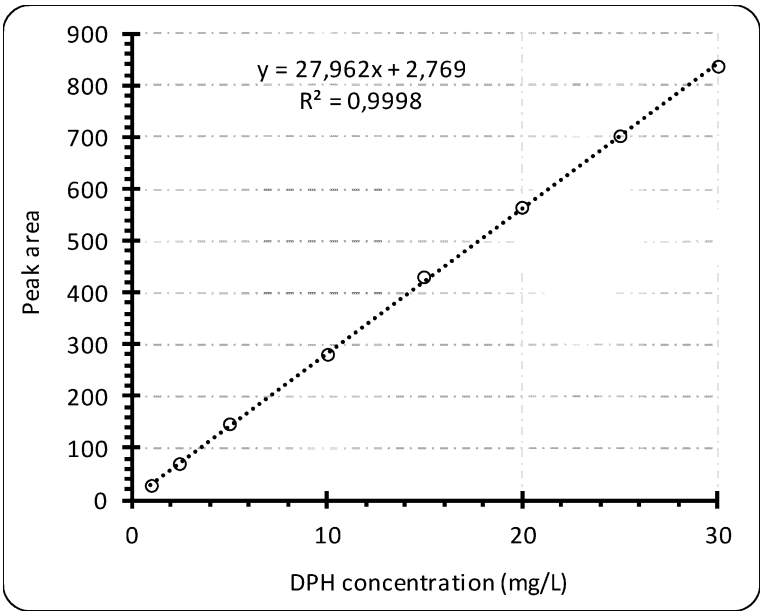

Figure 6. Calibration curve of DPH active ingredient.

Table 5. DPH loading capacities of all formulations.

Formulation	F1	F2	F3	F4	F5	F6
DPH loading capacity (mg/g)	97.1±7.7	56.2±1.1	54.8±2.4	85.5±3.8	48.8±1.8	51.3±5.6

3.4 In vitro DPH Release Profiles of the Formulations

The drug-loaded composite was added to the hard gelatin capsule to make the prepared product easier for the patient compliance. Orally used capsule formulations have high patient compatibility, ease of use, and low cost (Hadi et al., 2013). The *in vitro* release profiles of the DPH active ingredient were examined in gastric medium (pH 1.2) versus time with all formulations (Figure 7).

The basket method (USP Apparatus I) was used in the release studies of formulations filled into capsules. This method is a frequently used dissolution for capsule formulations (Kumar et al., 2012; Lo et al., 2013; Damian et al., 2021). As shown in Figure 7, with the disintegration of the capsule wall depending on the temperature and medium, the DPH passed into the release medium from the 5^{th} minute. This indicated that the capsule wall began to break down within 5 min. At the same time, this situation was observed observationally during the study.

The rapid release of the DPH from the carrier system to the release medium is related to the fact that DPH is an active ingredient with high solubility in water (Wang et al., 2017). Formulations without chitosan polymer (F1 and F4) showed faster and higher drug release from the 5^{th} minute than the other formulations. During the first 45 min, 50% or more of all formulations diffused rapidly to the release medium, followed by a slower release.

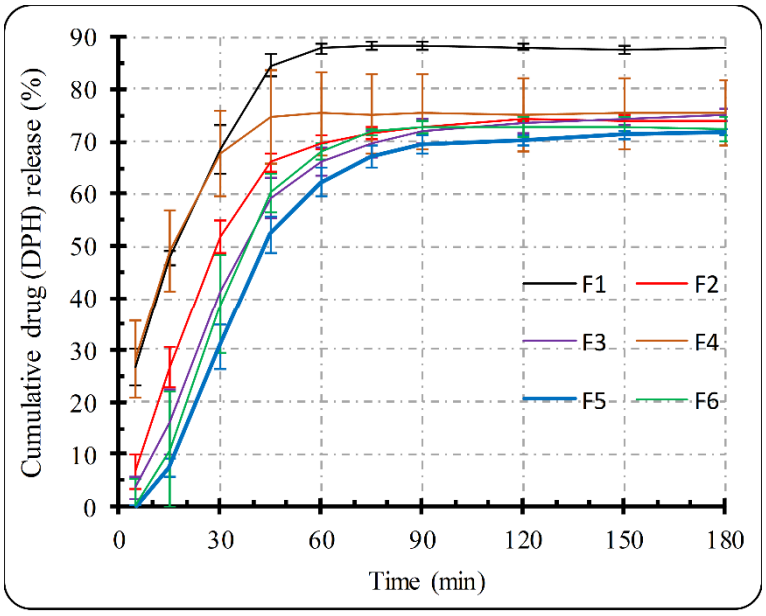

Figure 7. DPH release profiles of all composite formulations at pH 1.2.

F1 formulation showed statistically higher drug release at all-time points than chitosan-containing formulations (F2, F3, F5, F6) ($p<0.05$). The chitosan with bio-adhesive (Arpa et al., 2023) and binding properties (Tang et al., 2017) adsorbed on the surface and pores of the diatomite particles, causing the drug release to be slower than in other formulations.

When the chitosan-free F1 and F4 formulations were evaluated among themselves, a proportionally higher release amount was observed in F1 than in F4. This is related to the fact that there is a higher amount of carrier material (1/10 = DPH/Diatomide) in the F1 formulation than the active ingredient. In other words, while the amount of DPH in the environment during drug loading was the same, there was more diatomite in the F1 formulation. Thus, there was not enough driving force for DPH molecules to be adsorbed on micro and mesopores, and DPH molecules concentrated more rapidly in macropores. This facilitated the release of DPH molecules, allowing it to occur at a higher rate. In the F4 formulation, however, since there was less diatomite and relatively more driving force was provided, DPH molecules were allowed to move toward the micro and mesopores. This resulted in the inability of DPH molecules concentrated in the micropores and crevices to pass into the release medium completely. The same situation is seen in the F2 and F5 formulations.

As a result, the expression of repulsive force is the force that pushes the adsorbate toward the adsorbent surface and pores. A high level causes high adsorption and more adsorbate concentration in micropores/slits. High adsorbate (DPH) concentration in the environment or low adsorbent (diatomite) concentration provides the elevated driving force. However, no significant difference was observed between F3 and F6 in this respect ($p > 0.05$). The F5 formulation with less diatomite released less DPH in the first 60 min than the others. As a result of this situation, it can be understood that DPH accumulated in the inner pores at a higher rate, and the high speed of chitosan, however, caused the release to be less and slower. There was no significant difference between F3 and F6 formulations regarding release percentage and kinetics. From the 90th minute, the DPH release from all formulations finished.

3.5 In vitro Release Kinetics

Several different kinetic models were used to explain the DPH active ingredient release kinetics of the products of all formulations. Kinetic models were evaluated with the data obtained from drug release studies. The correlation coefficients (r^2) and "n" values obtained from the kinetic models are given in Table 6.

Table 6. The kinetic models used and the *in vitro* drug release parameters obtained.

Kinetic model / Formulation	Zero order (r^2)	First order (r^2)	Higuchi (r^2)	Hixson-Crowell (r^2)	Korsmeyer-Peppas (r^2)	Korsmeyer-Peppas n
F1	0.9261	0.8436	0.9997	0.8756	0.9922	0.4983
F2	0.9219	0.7654	0.9963	0.8307	0.9696	0.9611
F3	0.9653	0.8132	0.9734	0.8867	0.9853	1.2136
F4	0.9228	0.7634	0.9991	0.7896	0.9679	0.4137
F5	0.9823	0.7272	0.9634	0.8888	0.9902	1.6581
F6	0.9705	0.7204	0.9734	0.8779	0.9787	1.6813

As shown in Table 6, the kinetic with the highest r^2 values of the equations obtained from the release data was evaluated as the most appropriate. According to the findings, the model with the highest r^2 value was Higuchi kinetics in general. Higuchi is a mathematical kinetics determining the release rates of active ingredients dispersed in drug delivery systems which show controlled release. The findings and the prepared system's data showed that it was compatible with this kinetic. On the other hand, in Korsmeyer Peppas kinetics, where the data up to the point where the drug release reaches 70%, the slope of the equation, the "n" value, was used to interpret the release profiles. It indicates Fickian diffusion when $n \leq 0.5$ and non-Fickian diffusion when $0.5 < n$. In non-Fickian diffusion, the release of the active ingredient from the formulation occurs as a combination of both diffusion and erosion-controlled release (Coneac et al., 2015; Laxmi et al., 2015; Arpa et al., 2022). Therefore, the fact that the n value was less than 0.5 in F1 and F4 formulations that did not contain chitosan indicated that drug release occured by the Fickian mechanism. Adding chitosan to the formulations caused a change in the release characteristics. Formulations containing chitosan, $n>1$, indicated non-Fickian diffusion and zero-order kinetics. The fact that the zero-order kinetics have the highest r^2 values after the Higuchi kinetics means that the release of the active ingredient was time-independent. When the release data obtained were examined over the f2 similarity factor, the formulations that did not contain chitosan polymer (F1 and F4) did not show similarity both among themselves and in pairwise pairings with other formulations ($f2<50$). While the release data were similar in all pairwise comparisons of the four formulations containing chitosan ($f2>50$), only the F2 and F5 formulations had a similarity factor of 48.13 (dissimilar).

4. CONCLUSIONS

As a result of preliminary characterization tests (XRD, XRF) of the raw diatomite, it was determined that it mainly consisted of silicon dioxide. The broad flat peak detected in the XRD analysis proved that the raw diatomite sample was composed of amorphous silica. However, since it is known that organic impurities exist in raw diatomite ores, purification was carried out by the calcination process. Thus, both purer diatomite with higher surface area was successfully obtained.

It was determined that the presence of chitosan in the prepared DPH-loaded formulations caused a decrease in the DPH-loading capacity. The formulation with the highest DPH loading capacity was F1 (97.13 mg/g), and the formulation with the lowest loading capacity was F5 formulation (48.75 mg/g).

As a result of *in vitro* release studies, it was observed that formulations containing chitosan polymer (F2, F3, F5, F6) had slower release than other formulations. At the same time, it was determined that the F5 formulation, which has less diatomite content than other formulations, released less and slower DPH than other formulations. In this case, it was concluded that for the F5 formulation, the DPH active ingredient accumulated in the diatomite inner pores at a higher rate, and with the presence of chitosan, the release was both less and slower.

Drug release profiles of the prepared formulations were compatible with Higuchi kinetics. The n value in Korsmeyer Peppas kinetics was $n<0.5$ for formulations F1 and F4 (chitosan free), which was associated with the Fickian mechanism. In other formulations, this indicated non-Fickian diffusion and zero-order kinetics as $n>1$.

In conclusion, the study showed that diatomite-chitosan composites can have controlled release ability and be used as potential drug carrier systems. Formulations with a slower release profile can be obtained with more detailed studies, incredibly when enriching the diatomite and making it composite with chitosan. More effective drug formulations can be obtained by trying the compositions of other polymeric materials, either alone or together, with diatomite at different composition ratios.

5. ACKNOWLEDGEMENTS

This study was financially supported by Afyon Kocatepe University, Scientific Research Project (BAP), Project No: 23.FEN.BIL.05.

6. CONFLICT OF INTEREST

The authors declare that they have no known competing financial interests or personal relationships that could have appeared to influence the work reported in this paper.

7. AUTHOR CONTRIBUTION

Zeynep Özkan: investigation, writing, methodology, original draft. Muhammet Davut Arpa: original draft, methodology, writing, conceptualization. Melih Özçatal: methodology, editing, conceptualization. Hakan Çiftçi: supervision**,** writing, methodology, editing, conceptualization.

8. REFERENCES

Abbas H.K., AbdulRazzaq I.F., Salal Y.A., Shaheed D.Q., Preparation and evaluation of proniosomal gel containing diphenhydramine HCl, Drug Invention Today, 13(2), 2020.

Abdel-Bary A.S., Tolan D.A., Nassar M.Y., Taketsugu T., El-Nahas A.M., Chitosan, magnetite, silicon dioxide, and graphene oxide nanocomposites: Synthesis, characterization, efficiency as cisplatin drug delivery, and DFT calculations, International Journal of Biological Macromolecules, 154, 621-633, 2020.

Akyuz L., Kaya M., Koc B., Mujtaba M., Ilk S., Labidi J., Yildiz A., Diatomite as a novel composite ingredient for chitosan film with enhanced physicochemical properties, International journal of biological macromolecules, 105, 1401-1411, 2017.

Arpa M.D., Okur N.Ü., Gök M.K., Özgümüş S., Cevher E., Chitosan-based buccal mucoadhesive patches to enhance the systemic bioavailability of tizanidine, International Journal of Pharmaceutics, 123168, 2023.

Arpa M.D., Seçen İ.M., Erim Ü.C., Hoş A., Üstündağ Okur N., Azelaic acid loaded chitosan and HPMC based hydrogels for treatment of acne: formulation, characterization, in vitro-ex vivo evaluation, Pharmaceutical Development and Technology, 27(3), 268-281, 2022.

Arpa M.D., Ünükür M.Z., Erim Ü.C., Formulation, characterization and in vitro release studies of terbinafine hydrochloride loaded buccal films, Journal of Research in Pharmacy, 25(5): 667-680, 2021.

Arpa M.D., Yağcılar A.P., Biltekin S.N., Novel benzydamine hydrochloride and chlorhexidine gluconate loaded bioadhesive films for local treatment of buccal infections, Journal of Drug Delivery Science and Technology, 84, 104497, 2023.

Burkhanova N.D., Yugai S.M., Pulatova K.P., Nikononvich G.V., Milusheva R.Y., Voropaeva N.L., Rashidova S.S., Structural investigations of chitin and its deacetylation products, Chemistry of Natural Compounds, 36, 352-355, 2000.

Çiftçi H., Arpa M.D., Gülaçar İ.M., Özcan L., Ersoy B., Development and evaluation of mesoporous montmorillonite/magnetite nanocomposites loaded with 5-Fluorouracil, Microporous and Mesoporous Materials, 303, 110253, 2020.

Çiftçi H., Arpa M.D., Gülaçar İ.M., Özcan L., Ersoy B., Development and evaluation of mesoporous montmorillonite/magnetite nanocomposites loaded with 5-Fluorouracil, Microporous and Mesoporous Materials, 303, 110253, 2020.

Çiftçi H., Ersoy B., Evcin A., Purification of Turkish bentonites and investigation of the contact angle, surface free energy and zeta potential profiles of organo-bentonites as a function of CTAB concentration, Clays and Clay Minerals, 68, 250-261, 2020.

Coneac G., Vlaia V., Olariu I., Muţ A.M., Anghel D.F. Ilie C., Vlaia L., Development and evaluation of new microemulsion-based hydrogel formulations for topical delivery of fluconazole, Aaps Pharmscitech, 16, 889-904, 2015.

Damian F., Harati M., Schwartzenhauer J., Van Cauwenberghe O., Wettig S.D., Challenges of dissolution methods development for soft gelatin capsules, Pharmaceutics, 13(2), 214, 2021.

Ediz N., Bentli İ., Tatar İ., Improvement in filtration characteristics of diatomite by calcination, International Journal of Mineral Processing, 94(3-4), 129-134, 2010.

Fowler C.E., Buchber C., Lebeau B., Patarin J., Delacôte C., Walcarius A., An aqueous route to organically functionalized silica diatom skeletons, Applied surface science, 253(12), 5485-5493, 2007.

Gao B., Jiang P., An F., Zhao S., Ge Z., Studies on the surface modification of diatomite with polyethyleneimine and trapping effect of the modified diatomite for phenol, Applied surface science, 250(1-4), 273-279, 2005.

Gârea S.A., Mihai A.I., Vasile E., Nistor C., Sârbu A., Mitran R., Synthesis of new porous clay heterostructures: The influence of co-surfactant type, Materials Chemistry and Physics, 179, 17-26, 2016.

Gaware S.A., Rokade K.A., Kale S.N., Silica-chitosan nanocomposite mediated pH-sensitive drug delivery, Journal of Drug Delivery Science and Technology, 49, 345-351, 2019.

Ghebaur A., Garea S.A., Iovu H., New polymer–halloysite hybrid materials—potential controlled drug release system, International journal of pharmaceutics, 436(1-2), 568-573, 2012.

Gültürk E., Güden M., Thermal and acid treatment of diatom frustules, Journal of Achievements in Materials and Manufacturing Engineering, 46(2), 196-203, 2011.

Hadi A., Rao N.G., Rao A.S., Shiva G., Akram J.W., Impact of capsules as a carrier for multiple unit drug delivery and the importance of HPMC capsules, Research Journal of Pharmacy and Technology, 6(1), 34-43, 2013.

Ibrahim S.M., Bin Jumah M.N., Othman S.I., Alruhaimi R.S., Al-Khalawi N., Salama Y.F., Abukhadra M.R., Synthesis of chitosan/diatomite composite as an advanced delivery system for ibuprofen drug; equilibrium studies and the release profile, Acs Omega, 6(20), 13406-13416, 2021.

Kevadiya B.D., Patel T.A., Jhala D.D., Thumbar R.P., Brahmbhatt H., Pandya M.P., Bajaj H.C., Layered inorganic nanocomposites: a promising carrier for 5-fluorouracil (5-FU), European Journal of Pharmaceutics and Biopharmaceutics, 81(1), 91-101, 2012.

Kumar N., Sangeetha D., Sunil Reddy P., Malleswara Reddy A., Development and validation of a dissolution test for delayed release capsule formulation of duloxetine hydrochloride, Current Pharmaceutical Analysis, 8(3), 236-246, 2012.

Laxmi M., Bhardwaj A., Mehta S., Mehta A., Development and characterization of nanoemulsion as carrier for the enhancement of bioavailability of artemether, Artificial cells, nanomedicine, and biotechnology, 43(5), 334-344, 2015.

Lo L., Lu X., Lloyd D., Dissolution testing of a controlled-release capsule formulation: Challenges and solutions using a semi-automated dissolution system, Dissolut. Technol, 20(2), 6-12, 2013.

Luo H., Ji D., Li C., Zhu Y., Xiong G., Wan Y., Layered nanohydroxyapatite as a novel nanocarrier for controlled delivery of 5-fluorouracil, International Journal of Pharmaceutics, 513(1-2), 17-25, 2016.

Lv G., Chang P.H., Xing X., Jiang W.T., Jean J.S., Li Z., Investigation of intercalation of diphenhydramine into the interlayer of smectite by XRD, FTIR, TG-DTG analyses and molecular simulation, Arabian Journal of Chemistry, 10(6), 855-861, 2017.

M Rosenholm J., Sahlgren C., Linden M., Multifunctional mesoporous silica nanoparticles for combined therapeutic, diagnostic and targeted action in cancer treatment, Current drug targets, 12(8), 1166-1186, 2011.

Moradı A.N., Yıldız A., Seydiler (Afyonkarahisar) diyatomitleri ile modifiye edilmiş bitümlerin reolojik özelliklerinin araştırılması, Afyon Kocatepe University Graduate School of Natural and Applied Sciences, Master Thesis (Printed), 2021.

Queiroz M.F., Teodosio Melo K.R., Sabry D.A., Sassaki G.L., Rocha H.A.O., Does the use of chitosan contribute to oxalate kidney stone formation?, Marine drugs, 13(1), 141-158, 2014.

Rea I., Martucci N.M., De Stefano L., Ruggiero I., Terracciano M., Dardano P., Lamberti A., Diatomite biosilica nanocarriers for siRNA transport inside cancer cells, Biochimica et Biophysica Acta (BBA)-General Subjects, 1840(12), 3393-3403, 2014.

Reka, A.A., Pavlovski, B., Fazlija, E., Berisha, A., Pacarizi, M., Daghmehchi, M., & Oral, A., Diatomaceous Earth: Characterization, thermal modification, and application, Open Chemistry, 19(1), 451-461, 2021.

Rezaeifar M., Mahmoudvand H., Amiria M., Formulation and evaluation of diphenhydramine gel using different gelling agents, Der Pharma Chemica, 8(5), 243-9, 2016.

Ruggiero I., Terracciano M., Martucci N.M., De Stefano L., Migliaccio N., Tatè R., Rea I., Diatomite silica nanoparticles for drug delivery, Nanoscale research letters, 9, 1-7, 2014.

Silvestri S., Foletto E.L., Preparation and characterization of Fe2O3/TiO2/clay plates and their use as photocatalysts, Ceramics International, 43(16), 14057-14062, 2017.

Tang C., Hu D., Cao Q., Yan W., Xing B., Silver nanoparticles-loaded activated carbon fibers using chitosan as binding agent: Preparation, mechanism, and their antibacterial activity, Applied Surface Science, 394, 457-465, 2017.

Taş B., Çetin M., Biyolojik orijinli tek doğal mineral: diyatomit, Tübav Bilim Dergisi, 5(2), 28-46, 2012.

Thakur G., Singh A., Singh I., Formulation and evaluation of transdermal composite films of chitosan-montmorillonite for the delivery of curcumin, International journal of pharmaceutical investigation, 6(1), 23, 2016.

Tian L., Abukhadra M.R., Mohamed A.S., Nadeem A., Ahmad S.F., Ibrahim K.E., Insight into the loading and release properties of an exfoliated kaolinite/cellulose fiber (EXK/CF) composite as a carrier for oxaliplatin drug: cytotoxicity and release kinetics, ACS omega, 5(30), 19165-19173, 2020.

Tsai W.T., Lai C.W., Hsien, K.J., Characterization and adsorption properties of diatomaceous earth modified by hydrofluoric acid etching, Journal of Colloid and Interface Science, 297(2), 749-754, 2006.

Vilar G., Tulla-Puche J., Albericio F., Polymers and drug delivery systems, Current drug delivery, 9(4), 367-394, 2012.

Vona, D., Flemma, A., Piccapane, F., Cotugno, P., Cicco, S.R., Armenise, V., & Ragni, R., Drug delivery through epidermal tissue cells by functionalized biosilica from diatom microalgae, Marine Drugs, 21(8), 438, 2023.

Wang C., Hu S., Sun C.C., Expedited development of diphenhydramine orally disintegrating tablet through integrated crystal and particle engineering, Molecular pharmaceutics, 14(10), 3399-3408, 2017.

Wang Y., Cai J., Jiang Y., Jiang X., Zhang D., Preparation of biosilica structures from frustules of diatoms and their applications: current state and perspectives, Applied microbiology and biotechnology, 97, 453-460, 2013.

Wu X.J., Wang J.D., Cao L.Q., Characterization and adsorption performance of chitosan/diatomite membranes for Orange G removal, e-Polymers, 16(2), 99-109, 2016.

Yang, H., Ma, Z., Guan, X., Xiang, Z., Ke, Y., Xia, Y., & Yin, J, Facile fabrication of diatomite-based sponge with high biocompatibility and rapid hemostasis, Journal of Applied Polymer Science, 138(46), 51360, 2021.

Yusan S., Gok C., Erenturk S., Aytas, S., Adsorptive removal of thorium (IV) using calcined and flux calcined diatomite from Turkey: Evaluation of equilibrium, kinetic and thermodynamic data, Applied Clay Science, 67, 106-116, 2012.

Yusan S., Korzhynbayeva K., Aytas S., Tazhibayeva S., Musabekov K., Preparation and investigation of structural properties of magnetic diatomite nanocomposites formed with different iron content, Journal of Alloys and Compounds, 608, 8-13, 2014.

Zargarian S.S., Haddadi-Asl V., Hematpour H., Carboxylic acid functionalization of halloysite nanotubes for sustained release of diphenhydramine hydrochloride, Journal of Nanoparticle Research, 17, 1-13, 2015.

Zhang H., Shahbazi M.A., Mäkilä E.M., da Silva T.H., Reis R.L., Salonen J.J., Santos H.A., Diatom silica microparticles for sustained release and permeation enhancement following oral delivery of prednisone and mesalamine, Biomaterials, 34(36), 9210-9219, 2013.

Zheng Y., Fang H., Wang F., Huang H., Yang J., Zuo, G., Fabrication and characterization of mesoporous Si/SiC derived from diatomite via magnesiothermic reduction, Journal of Solid State Chemistry, 277, 654-657, 2019.

Zheng Y., Wang A., Enhanced adsorption of ammonium using hydrogel composites based on chitosan and halloysite, Journal of Macromolecular Science, Part A, 47(1), 33-38, 2009.